Article:
SANDERSON, P N, Su, Dang Sheng, Chang, I T H et al. (4 more authors) (2016) Characterisation of iron-rich atmospheric submicrometre particles in the roadside environment. Atmospheric Environment. pp. 167-175. ISSN: 1352-2310

https://doi.org/10.1016/j.atmosenv.2016.05.040

Atmospheric Environment 140 (2016) 167–175

Contents lists available at ScienceDirect

Atmospheric Environment

journal homepage: www.elsevier.com/locate/atmosenv

Characterisation of iron-rich atmospheric submicrometre particles in the roadside environment

P. Sanderson [a], S.S. Su [b, 1], I.T.H. Chang [b], J.M. Delgado Saborit [a], D.M. Kepaptsoglou [c], R.J.M. Weber [d], Roy M. Harrison [a, *]

[a] School of Geography, Earth and Environmental Sciences, University of Birmingham, Edgbaston, Birmingham, B15 2TT, United Kingdom
[b] School of Metallurgy and Materials, University of Birmingham, Edgbaston, Birmingham, B15 2TT, United Kingdom
[c] SuperSTEM, SciTech Daresbury Campus, Keckwick Lane, Daresbury, WA4 4AD, United Kingdom
[d] School of Biosciences, University of Birmingham, Edgbaston, Birmingham, B15 2TT, United Kingdom

HIGHLIGHTS

- Airborne particles sampled with nano-MOUDI impactor.
- Many particles with high and moderate Fe content.
- Clusters comprised of primary particles of 20–30 nm diameter.
- Iron oxides are identified by TEM-EELS and are externally mixed.

ARTICLE INFO

Article history:
Received 17 February 2016
Received in revised form
12 May 2016
Accepted 23 May 2016
Available online 24 May 2016

Keywords:
Iron oxide
Nanoparticles
Ultrafine particles
Roadside
Metallic

ABSTRACT

Human exposure to ambient metallic nanoparticles is an area of great interest owing to their potential health impacts. Ambient metallic nanoparticles found in the roadside environment are contributed by combustion engines and wear of brakes, tyres and road surfaces. Submicrometre atmospheric particles collected at two UK urban sites have been subject to detailed characterisation. It is found that many metallic nanoparticles collected from roadside sampling sites are rich in iron. The Fe-rich nanoparticles can be classified into (1) high Fe content (ca 90 wt%) with each alloying element less than 1 wt%; and (2) moderate Fe content (<75 wt%) with high manganese and silicon content. Both clusters contain a variable mix of minor constituents, Mn, S and Si being most important in the high-Fe group. The moderate Fe group also contains Zn, Cu, Ba, Al and Ca. The Fe-rich nanoparticles exhibit primary particle sizes ranging between 20 and 30 nm, although some much larger particles up to around 100 nm can also be observed, along with some very small particles of 10 nm or less. These tend to agglomerate forming clusters ranging from ~200 nm to 1 μm in diameter. The iron-rich particles observed are oxides, taking the form of spheres or multifaceted regular polyhedra. Analysis by EELS shows that both high- and moderate-Fe groups include particles of FeO, Fe_3O_4, α-Fe_2O_3 and γ-Fe_2O_3 of which γ-Fe_2O_3 is the most prominent. Internal mixing of different Fe-oxides is not observed.

1. Introduction

Iron is often present in substantial concentrations in airborne particulate matter (e.g. Harrison et al., 2004). This is significant because iron rich particles exert an important role in some atmospheric chemical reactions, including the oxidation of S(IV) compounds such as SO_2 to S(VI) compounds such as H_2SO_4 (Grgić et al., 1996), and on biogeochemical cycles – deposition of atmospheric iron influences marine productivity and therefore has a marked influence on the global carbon cycle (Mahowald et al., 2005).

Atmospheric iron is also known to have adverse effects on human health, being associated with inflammation and DNA damage via oxidative stress caused by generation of free radicals and

* Corresponding author. Department of Environmental Sciences/Center of Excellence in Environmental Studies, King Abdulaziz University, PO Box 80203, Jeddah, 21589, Saudi Arabia.
E-mail address: r.m.harrison@bham.ac.uk (R.M. Harrison).
[1] Now at: Materials Science and Engineering Department, Texas A&M University, Texas, USA.

http://dx.doi.org/10.1016/j.atmosenv.2016.05.040
1352-2310/

reactive oxygen species (Gurzau et al., 2003). As the population are exposed to inhalable atmospheric iron from many sources, and given that iron is known to be biologically active and potentially harmful, its presence is a public health concern. Establishing the physical and chemical characteristics of the atmospheric iron burden, such as size distribution, particle morphology, chemical composition and oxidation state will therefore underpin assessments of the risks to human health from exposure.

Iron in atmospheric particulate matter originates from a number of crustal and anthropogenic sources (Sanderson et al., 2014). These include industrial and metallurgical processes (Buonanno et al., 2011; Cernuschi et al., 2012; Reinard et al., 2007), combustion of fossil fuels (Linak et al., 2007), emissions from transport sources such as diesel emissions (Liati et al., 2012; Patel et al., 2012), tyre wear (Adachi and Tainosho, 2004), brake wear (Kukutschová et al., 2011), shipping (Moldanová et al., 2009) and resuspension of crustal materials and road dust (Amato et al., 2011). Use of iron compounds as catalytic additives in automotive engines will also lead to emissions of iron. Although these reduce the total particulate emission from the engine, metallic oxides have been reported to be included in the soot emitted when such additives are used (Lee et al., 2006; Song et al., 2006).

Moreover, each of these sources contributes iron with differing physical and chemical properties resulting from the effect of their different formation processes. Previously reported examples include nanoparticulate γ-Fe_2O_3 from fly ash (Linak et al., 2007), nanoparticulate Fe_3O_4 from in-cylinder melting of engine wear fragments (Liati et al., 2015), various oxides, silicates and W and Cr alloys from waste-to-energy plants (Buonanno et al., 2011) and agglomerates of nanoparticles of Fe_2O_3 and Fe_3O_4 from brake discs and pads (Kukutschová et al., 2011).

The project was established with a view to characterisation of metallic nanoparticles, with a particular interest in Fe because of its apparent biological activity (Zhou et al., 2003; Mahmoudi et al., 2012) and cerium which is used as a nano-particulate motor fuel additive, hence requiring evaluation of its environmental and human health consequences. Our results for cerium have been published elsewhere (Gantt et al., 2014, 2015). This paper aims to present comprehensive characterisation data for submicrometre atmospheric iron particles collected at two UK urban sites, including physical structure and morphology, and chemical composition, using analytical Transmission Electron Microscopy (TEM) techniques; namely Energy Dispersive Spectroscopy (EDS) and oxidation state data from Electron Energy Loss Spectroscopy (EELS). These are all important parameters influencing the interaction of these particles with biological systems.

2. Methodology

2.1. Details of sampling sites

Samples for electron microscope analysis were collected at two sampling sites in urban locations:

Bristol Road Observatory: This site is a traffic roadside site located at the South Entrance to the University of Birmingham campus, Edgbaston, adjacent to the A38 main road (approximately 4 m distance). Size segregated bulk filter samples and samples for TEM were collected here by nanoMOUDI. There is a large four-way intersection adjacent to the site controlled by traffic lights – consequently the traffic is frequently stopped directly adjacent to the sampling location. The most recent figures from the Department for Transport record an average annual daily flow (AADF) of 27,265 vehicles in 2011. HGVs account for 1.46% of this traffic and buses/coaches 2.4%. The site is slightly elevated relative to the road so the inlet was approximately 3–4 m above the road surface.

Newcastle Civic Centre: The Automatic Urban and Rural Network (AURN) station at Newcastle Civic Centre, Newcastle-upon-Tyne was used as a traffic roadside site to collect nanoMOUDI and MOUDI bulk filter and TEM grid samples. The site was chosen because Newcastle's public buses are run by a company which used cerium oxide fuel additives (Envirox) in their fleet in this area at the time of sampling. The physical and chemical composition of these samples would therefore make a useful comparison to the site in Birmingham, where cerium oxide additives are not used by the major local transport operators. No traffic flow data are available for the site.

2.2. Sample collection procedures

A nanoMOUDI-ii 125R cascade impactor (MSP Corporation) was used to collect size resolved particulate matter samples. The instrument has thirteen stages with nominal 50% cut-points of 10,000, 5600, 3200, 1800, 1000, 560, 320, 180, 100, 56, 32, 18 and 10 nm when operated at an inlet flow rate of 10.0 L/min. The impactor was paired with a Leybold SV 16 rotary vane oil pump in Newcastle, and a slightly more powerful SV 25 pump in Birmingham, although the difference in flow-rate between these pumps was negligible; the TEM samples were collected at ~9.5 L/min in both cases, which would make minimal difference to the stated cut-points.

The instrument separates particles into a series of logarithmically equal size fractions based on atmospheric diameter, by accelerating particles through a fine jet and impaction upon a filter substrate mounted below on a rotating plate which collects the heavier particles while the lighter ones follow in the gas streamline to the next stage. In practice the cut-off diameters can be affected by particle bounce and particle blow-off leading to larger than expected particles being detected in the lower stages. Some evidence of this has been seen in these samples.

The experimental set-up at the sampling sites had the impactor and pump housed in a cabinet, with an inlet at the top of the housing covered by a rain hood. Two fans were positioned next to the pump to keep it as cool as possible during operation, but nevertheless temperatures in the region of 40–45 °C during operation were still recorded, particularly during the summer months. This would have the effect of reducing the mass of semi-volatile material collected by this method in bulk samples, requiring long collection times.

TEM samples were collected by affixing conventional 3 mm copper support grids, with lacey or ultra-thin carbon films, to aluminium filter substrates, then sampling at the normal rate for the instrument. Sampling at Newcastle was carried out using one set of films over three sessions totalling 8 h which was found to give suitable particle number density on the smaller stages below 180 nm. The 2014 Birmingham samples were initially collected for three hours; this proved inadequate despite the higher concentrations at this site, so they were reloaded and sampled for an additional three hours. At both sites sample collection was carried out in the afternoon. The trade-off for getting useful particle numbers in the ultrafine/pseudo-ultrafine range was that particles in the fine and coarse range were somewhat too dense, with particles overlaying each other on the grid surface. However, the analysis of submicron particles was the priority of the project. In both cases samples were collected outside rush-hour in cold winter weather. The data presented in this paper derive from comprehensive evaluation of one nano-MOUDI sample per site, collected over three separate afternoons.

2.3. TEM-X-EDS analysis

TEM imaging of samples was carried out using a Tecnai F20 Transmission electron microscope. For identifying likely particles the scanning (STEM) mode of the instrument was used in conjunction with high angle annular dark field (HAADF) imaging. Single particle chemical analysis was carried out using EDS, using an Oxford Instruments detector with ZAF quantification.

2.4. EELS analysis

STEM-EELS experiments were carried out using the Nion UltraSTEM™100 aberration-corrected dedicated STEM, equipped with a Gatan Enfina spectrometer. The microscope was operated at 100 kV acceleration voltage with a convergence angle of 30 mrad, corresponding to a probe size ~0.9 Å probe (full width at half-maximum). Commercially available Fe oxide standards were used to compare to the ambient particulate samples and thereby confirm the valence states. Further detail is given in the Supplementary Information.

2.5. ICPMS analysis

Filter samples were subjected to an acid leaching extraction procedure based on the method described by Harper et al. (1983) and used for several previous studies relating to brake wear particles (Gietl et al., 2010; Harper et al., 1983; Harrison et al., 2012). This used a reverse aqua regia solution prepared by mixing 66 mL HCl with 189 mL HNO_3 and made up to 1000 cm^3 with 18.2 MΩ deionised water. The filters were placed in 4 mL Nalgene vials and immersed in 2 mL of the extract solution, then heated to 100 °C in a water bath for 30 min, then sonicated at 50 °C for 30 min. The heating and sonicating steps were repeated, before the extract was transferred to a clean 30 mL vial and the extract vial washed with 4 mL deionised water twice, which was also transferred to the 30 mL vial to make up a total solution of 10 mL. Samples were stored at 5 °C prior to analysis.

Analysis was carried out on an Agilent 7500ce ICP-MS with an Octopole reaction system (ORS) which is used to remove polyatomic interferences such as ArO at mass 56 (Fe). The plasma runs with an RF power of 1500 W. A Miramist nebuliser is used for sample introduction. Detection limits are approximately 10 times lower than the reporting limits i.e. the detection limit for Fe is about 0.05 ng cm^{-3} giving a reporting limit of <0.5 ng cm^{-3} in solution. For a typical nanoMOUDI 7-day air sample (~90 m^3) this equates to 0.055 ng m^{-3} in air.

2.6. Data processing and visualisation methods

A distance matrix was calculated for the combined Birmingham and Newcastle datasets. Hierarchical cluster analysis was then employed to visually inspect the similarity between EDX elemental weight percentage data.

3. Results and discussion

3.1. Particle size distributions

Mass size distributions collected at the Birmingham roadside site demonstrated that particles in the 320–560 nm size range were highly abundant (see Fig. 1), which led to a decision to prioritise this size fraction.

ICP-MS analysis of nanoMOUDI samples from the Birmingham roadside site showed that Fe was the most abundant metal, as shown in Fig. 2. The mass-size distribution of Fe is illustrated in Fig. 3.

The bulk of the Fe is in particles above 1 μm aerodynamic diameter, but is not the focus of this study, which aims to characterise submicron particles. Iron is clearly present in the submicron fraction, in particular the 320–560 nm and 560–1000 nm size ranges.

3.2. Particle classification by cluster analysis

Cluster analysis was performed on the combined Newcastle and Birmingham roadside datasets to classify the collected particles by the weight percentage of each detected element, once elements associated with the grid (Cu, Au, C, O) had been subtracted.

The clustering of the SEM-EDX data revealed two major classes of iron-dominated particles (not including particles where another metallic element such as Pb was dominant): a high-Fe type (Fe ca. 90%/wt) (Fig. 4) and a moderate-Fe type (Fe ca. 75%/wt) which contained a much higher proportion of Mn and Si (Fig. 5). The mean composition of these classes varied slightly between the two sites, but the pattern was generally similar and so this may not be highly significant. The data from which the pie charts are constructed appears in Tables S2 and S3.

The particles clustered into the high-Fe group consist of on average 91.4% Fe by weight, with a variable composition of minor and trace constituents together totalling slightly less than 10% by weight. Mn, Si and S are the most important of these constituents. Most of these elements are either associated with crustal origin or with abrasive emissions (road dust and tyre wear components), but some elements do appear for which exhaust emissions are likely sources in this size range. Ni and Zn in this size fraction are likely to be related to traffic exhaust. A variety of sources are probably represented by these elements.

The average composition of the moderate-Fe cluster showed a much lower weight percentage of Fe, with Mn and Si being the most important minor constituents, followed by Zn. Many of the same elements are classified among the trace constituents found in this cluster (not all present in every particle). Two rare earth elements (La and Ce) appear in this cluster. Cu and Ba appear as trace constituents. Some crustal/resuspension elements (Al, Ca, La) appear too. Zn is more prominent than in the high-Fe group.

There are some differences between the two sites. At Newcastle the high-Fe type represented 70% of the sampled Fe-rich particles. At the Birmingham Roadside site, this figure is 48%. Fe content in this cluster is slightly higher in Birmingham than in the corresponding class for Newcastle – 96.0% compared to 89.9%. Many of the trace elements are the same but Ba, Al and Ca were not detected in the Newcastle high-Fe cluster.

A wider range of trace constituents were found at both sites in the moderate-Fe-Mn cluster compared to the high-Fe cluster, but Mn and Si are still the principal alloy elements. Fe content is again slightly higher in Birmingham than in the corresponding Newcastle cluster – 74% compared to 70%. This cluster incorporates both combustion (Ce) and brake wear (Cu, Ba) associated elements.

The high-Fe cluster in the Newcastle samples had fewer detectable trace components than that of the Birmingham samples (see Table 1). Unlike the latter, it contains Cr, but the most important minor constituents are still Mn/Si/S. The moderate-Fe group at Newcastle also contained fewer minor elements than the Birmingham group. Si and Mn were present in similar proportions to the Birmingham particles, but Zn was more prominent at Newcastle.

Both particle groups at both sites contain an interesting mix of elements. The common local source at both sites is traffic and most of the elements in these clusters are known to be associated with vehicle emissions. Fe, the dominant element in these samples, is

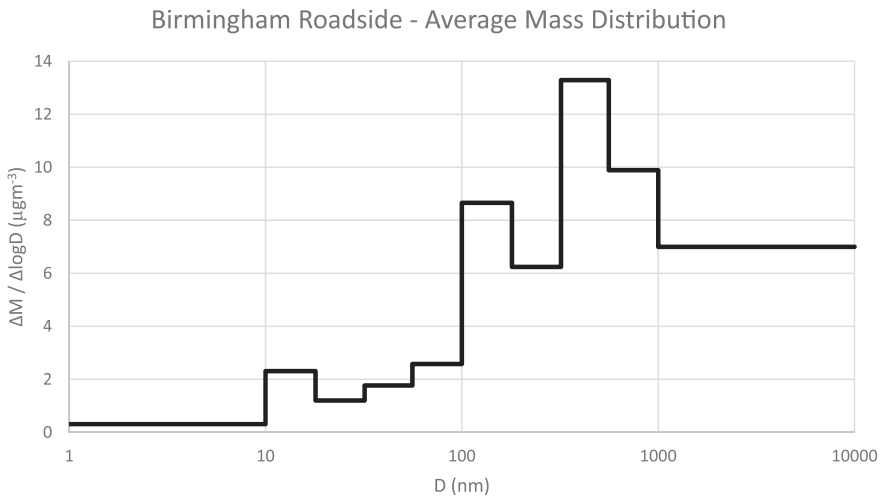

Fig. 1. Total particle mass-size distribution at roadside site in Birmingham (average of 10 samples of 7 days each).

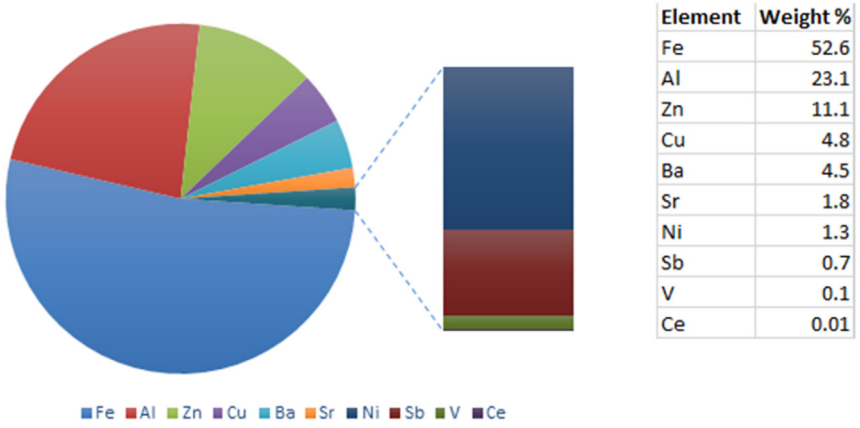

Element	Weight %
Fe	52.6
Al	23.1
Zn	11.1
Cu	4.8
Ba	4.5
Sr	1.8
Ni	1.3
Sb	0.7
V	0.1
Ce	0.01

Fig. 2. Pie chart showing abundance of the analysed metals (PM_{18}) as a percentage of the sum of masses of those metals (ICP-MS data).

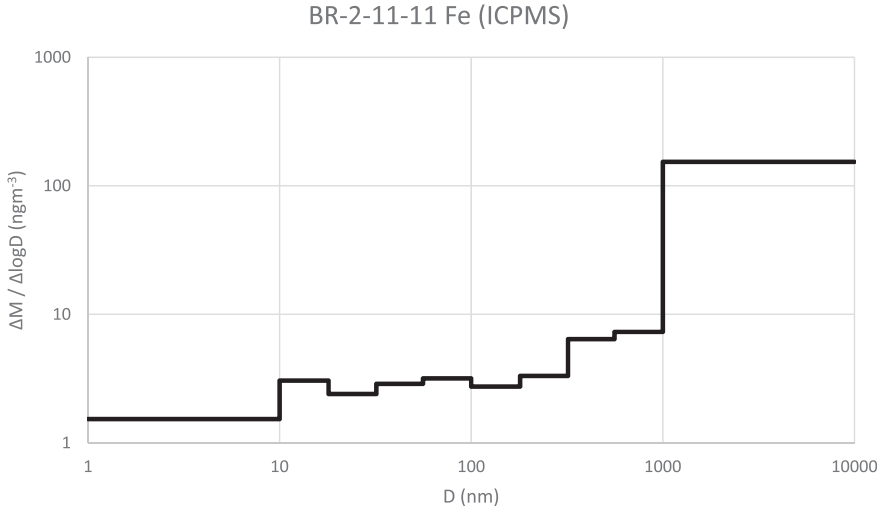

Fig. 3. Iron size distribution in sample collected at Birmingham Roadside analysed by ICP-MS, dated 2/11/11.

associated mainly with wear from brake components, both pads and rotors although recent results published by Liati et al. (2015) confirm that wear to engine components is also an important source, and the particles produced in that process are similar in many ways to the ones reported here (Liati et al., 2015). Brake wear is also the main source of Cu, Sb and especially Ba in roadside

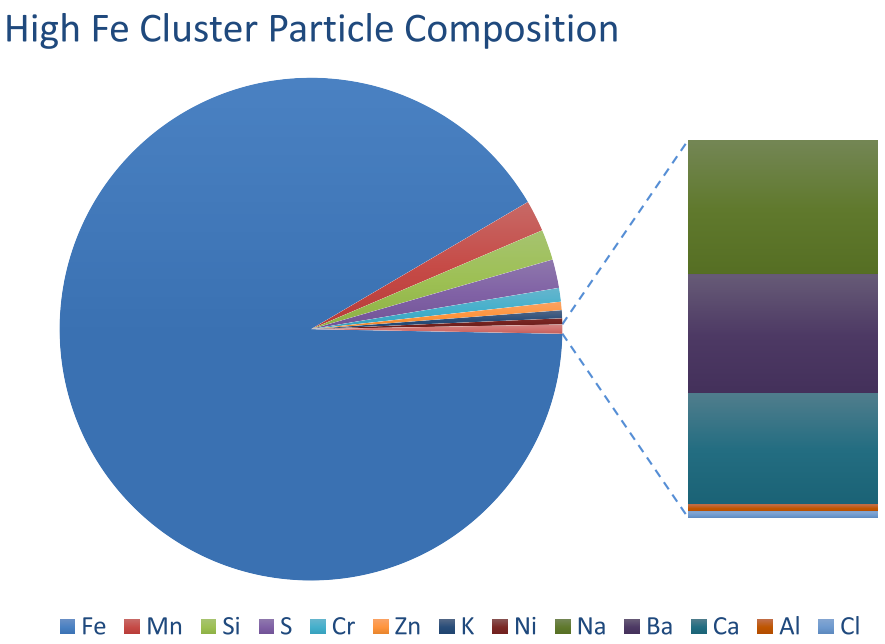

Fig. 4. Pie chart average of High-Fe particle composition from EDX weight percentage data (Table S2), both roadside sites combined (n = 48).

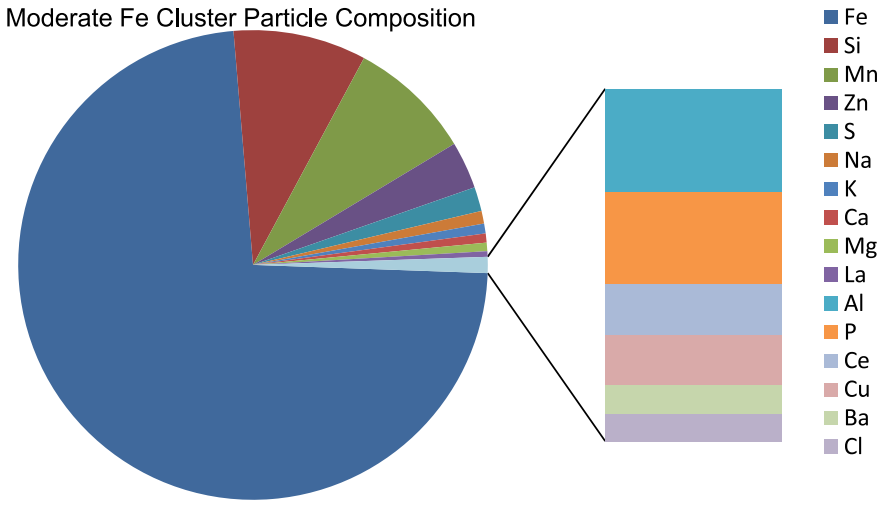

Fig. 5. Pie chart of average composition of moderate -Fe particle group from EDX weight percentage data (Table S3), both roadside sites combined (n = 28).

environments (Thorpe and Harrison, 2008). Zn is associated with multiple sources, including tyres, brakes and exhaust emissions from trace levels in lubricating oils (Thorpe and Harrison, 2008). Al and Ca are associated with crustal origins, but in particles in this size range it is likely that lubricating oils in engines are responsible, at least for Ca (Harrison et al., 2004).

3.3. Oxidation states

In previous studies it has generally been found that Fe(III) is the predominant oxidation state among atmospheric iron particles, although the picture is complicated because Fe participates in reactions with organic compounds which can lead to the reduction of Fe(III) (Erel et al., 1993). Fe and Mn are prone to undergo oxidation reactions during atmospheric transport and smaller particles are more likely to be found at higher oxidation states which have been found to have an average state between Fe(II) and (III) (Marris et al., 2013). A 2009 study on simulated atmospheric aging of Fe-Cr-Mn particles by Nico et al. (2009) reported that Mn in mixed metallic particles had the effect of capturing oxidative potential and passing it on to other components, leading to enhanced oxidation of Fe and Cr (Nico et al., 2009). The results presented in Fig. 6 support this contention, as a higher proportion of the Fe-Mn mixed particles are in the more oxidised states compared to the high-Fe type.

Our data confirm the presence of Fe(II) and (III) oxides, with Fe(III) being much more frequently observed. Analysis by EELS showed that both high- and low-Fe groups include particles of FeO, Fe_3O_4, α-Fe_2O_3 and γ-Fe_2O_3 of which γ-Fe_2O_3 is the most numerous in both groups, FeO being much less abundant than the other forms (see Fig. 6).

Forty-six EELS spectra were collected from two grids collected concurrently in Birmingham. Grid areas were randomly selected and likely particles in these areas were identified visually. Although the number of spectra and the sampled areas of the grid are small,

Table 1
Table of elemental weight percentage data from EDX (n.d. denotes not detectable).

High-Fe				Fe-Mn			
Element	Combined	Bham	Newcastle	Element	Combined	Bham	Newcastle
Fe	91.44	96.04	89.91	Fe	73.11	74.29	72.08
Mn	1.97	0.38	2.50	Si	9.17	8.42	9.82
Si	1.92	0.79	2.30	Mn	8.54	9.48	7.72
S	1.80	0.68	2.18	Zn	3.26	1.07	5.16
Cr	0.87	n.d.	1.15	S	1.66	1.10	2.15
Zn	0.53	0.42	0.56	Na	0.87	n.d.	1.63
K	0.50	0.15	0.62	K	0.68	n.d.	1.27
Ni	0.39	0.05	0.50	Ca	0.63	1.35	n.d.
Na	0.21	n.d.	0.28	Mg	0.58	1.24	n.d.
Ba	0.18	0.73	n.d.	La	0.38	0.83	n.d.
Ca	0.17	0.68	n.d.	Al	0.33	0.70	n.d.
Al	0.01	0.05	n.d.	P	0.29	0.41	0.18
Cl	0.01	0.04	n.d.	Ce	0.16	0.35	n.d.
				Cu	0.16	0.33	n.d.
				Ba	0.09	0.20	n.d.
				Cl	0.09	0.18	n.d.

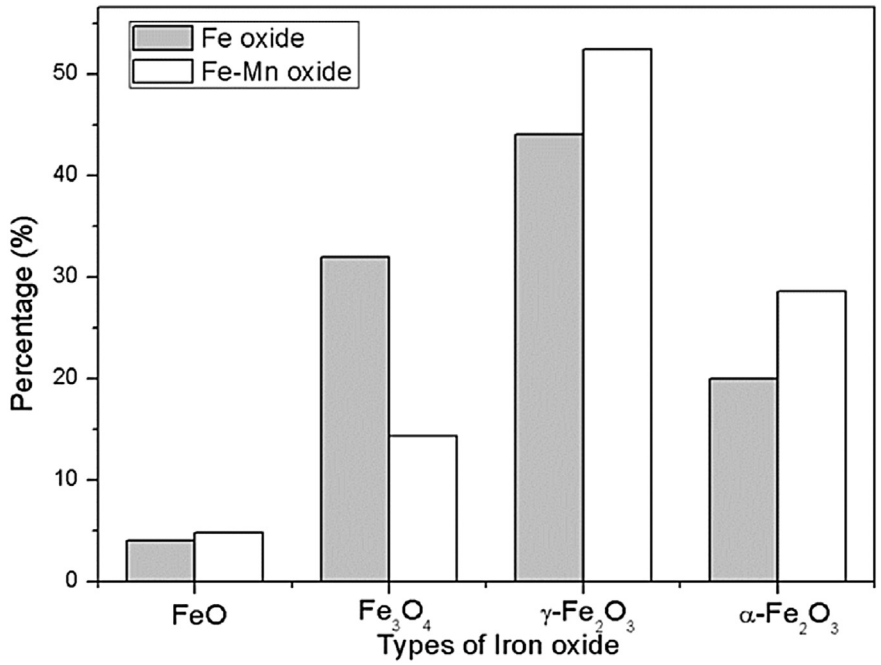

Fig. 6. Percentage of total number of spectra (n = 46) assigned by EELS to each oxidation state, for both particle groups (Samples collected at Birmingham Roadside).

the selection of sampling area is random and therefore results may be considered representative of the Fe particles. Of these spectra, there were 25 spectra taken from the high-Fe and 21 from the moderate −Fe groups. γ-Fe_2O_3 is the most frequently observed oxidation state in both composition types accounting for 45% of the Fe-Mn spectra and just over 50% of the Fe spectra. Fe_3O_4 accounts for a far greater proportion (>30% compared to < 15%) of the spectra from the high-Fe group than the moderate-Fe group. α-Fe_2O_3 accounts for around 25% of each particle class − a slightly higher percentage in the moderate-Fe group and slightly lower in the high-Fe group. FeO is the least common accounting for around 5% of each particle class.

The ratio of Fe (II): Fe_{total} in our EELS data is 0.043. This is at the lower end of the ratios measured in fog and cloud water at two sites in the Los Angeles basin by Erel et al. (1993), which varied between 0.02 and 0.55 (Erel et al., 1993). Other previous studies are also in agreement. d'Acapito et al. (2014) reported that Fe (II) was below detection limits of X-ray absorption spectroscopy (less than 5% of total Fe) in urban $PM_{2.5}$ and Fittschen et al. (2008) also found Fe (II) at similar levels across four size fractions from 15 nm to 16 μm (d'Acapito et al., 2014; Fittschen et al., 2008).

Kukutschová et al. (2011) reported that Fe was the dominant metallic element in ultrafine brake wear particles occurring primarily as agglomerates formed from nanoparticles of 20 nm upwards. In terms of particle size and structure these features are similar to the environmental particles we describe. Nanoparticle generation was reported to be negligible when the friction interface was cold, but became highly significant at rotor temperatures above 300 °C. Diffraction analysis showed the presence of Fe_3O_4 (magnetite) as well as both γ-Fe_2O_3 and α-Fe_2O_3 in these nanoparticles (Kukutschová et al., 2011).

By comparison, Liati et al. (2015) made observations of engine-derived agglomerated nanoparticles which only included Fe_3O_4, which was attributed to the short residence times of the primary

particles in the high-temperature environment not allowing the slower formation of the more stable Fe_2O_3 structures (Liati et al., 2015). However, these particles also bear a morphological resemblance to the ambient particles observed in this study, opening the possibility that particles of a similar type are being sampled in the environment having undergone oxidation post-emission.

Nanoparticulate γ-Fe_2O_3 is reported to be a prominent constituent of <500 nm diameter fly ash from coal burning (Linak et al., 2007). Reinard et al. (2007) also stated that iron is present in fly ash of all size ranges, including ultrafine ash in the form of nanoparticulate γ-Fe_2O_3. These particles are often associated with carbonaceous soot and are assumed to have formed through the oxidation of FeS_2 during combustion (Reinard et al., 2007).

Bardelli et al. (2011) reported that the iron speciation in road dust samples collected from the Traforo del San Bernando tunnel was dominated by the Fe_3O_4 and $FeCl_3$ forms, attributed respectively to exhaust emissions and salt to prevent icing on the road. Zhang et al. (2014), analysing fine particulates in Shanghai, reported that high levels of iron oxides (assumed to be principally Fe_2O_3, Fe_3O_4 and FeO(OH)) were associated with periods where emissions from iron/steel metallurgical sources were impacting on the sampling site. Using Mossbauer Spectroscopy, a study in Zakopane, Poland distinguished bulk crustal iron compounds (pyroxene, hematite and sulphides) and anthropogenically sourced ultrafines (oxides and oxyhydroxides). Urban aerosol was found to be dominated by local sources. Iron oxides and hydroxides (mostly α-Fe_2O_3 with some Fe_3O_4) were present all year round and an automotive source inferred. During winter, iron sulphides attributed to domestic coal-burning were also reported (Kopcewicz and Kopcewicz, 2001).

As shown in Tables 2 and 3, there is not a clear relationship between size and oxidation state, either for the Fe oxide particles, or for those which also contain Mn. Previous studies have indicated that smaller primary particles are associated with higher oxidation states, owing to the greater surface area relative to volume available to react with oxidising gases in the atmosphere (Marris et al., 2013). The small sample size, especially for FeO and Mn-alloyed Fe_3O_4, makes it difficult to draw any statistically robust conclusion from our data.

There is considerable variability of size and shape of both primary particles and agglomerates in the dataset. For the most part, the iron particles observed appear to be oxides, taking the form of spheres or multifaceted regular polyhedra, as can be seen in images 7(a) and 7(c). The primary particles are mainly in the range of 20–40 nm although some much larger particles up to around 100 nm can also be observed, along with some very small particles of 10 nm or even less. As can be seen in Fig. 7, the primary particles in the high-Fe group have a smaller median diameter, along with a bimodal distribution in which the main peak occurs at 20 nm and a much smaller second peak at 60 nm. This feature is not shared by the moderate-Fe group, in which the distribution curve is broader peaking at a higher diameter. They also agglomerate readily, forming irregular agglomerates of many primary particles. The agglomerated particle in Fig. S1(b) illustrates these features well.

Fig. S1 illustrates typical particles of both types and shows how similar the physical appearance of the two types is. In both cases a large number of spherical and near-spherical primary nanoparticles form irregular agglomerates in excess of 200 nm diameter. Primary nanoparticle size can be somewhat variable in both cases but is generally 20–40 nm. The particle shape is indicative of a high-temperature formation process.

Kukutschová et al. (2011) reported that Fe was the dominant metallic element in ultrafine and submicron brake wear, primarily as agglomerates formed from nanoparticles of 20 nm upwards. Such agglomerates would be similar to the observed environmental particles, but smaller particles can also be observed in some agglomerates. From this source, nanoparticle generation was reported to be negligible when the friction interface was cold, but became highly significant at rotor temperatures above 300 °C. Mosleh et al. (2004) reported that a population of particles rich in Fe, C and O was generated with an approximate average diameter of 350 nm, this composition showing the particles were generated from the cast-iron disc (Mosleh et al., 2004). This class was not dependent on sliding speed or load, which suggests that the formation process is temperature-dependent rather than load dependent. The approximate agglomerate size and composition would fit with the particles observed in the environment.

Liati et al. (2015) reported that Fe_3O_4 nanoparticles generated by melting and recooling of engine wear fragments were mostly 40–60 nm in diameter for spheres, but smaller particles showing cubic structures were also in evidence. These often appeared rounded at the edges but not spherical, possibly caused by heating (Liati et al., 2015). The particles reported by Liati et al. (2015) bear many morphological similarities to those we report although the size distributions are not identical.

Iron has also been detected in ultrafine particle emissions from a waste-to-energy plant as amorphous alloys with W and Cr, and in oxides (rounded, aggregated and suspended on phyllosilicates) which sometimes included one or both of these elements (Buonanno et al., 2011). Iron silicates with Al and Cr were also detected at the stack. Al and Cr are present in both particle classes we report but are not prominent, being only trace constituents. W was not observed in any of the particles which were analysed. Chen et al. (2006) report that iron-rich particles are an abundant component of airborne metals. Using electron diffraction, they demonstrated the presence of hematite. Iron was also found in combination with minor amounts of other metals typically manganese and zinc (Chen et al., 2006).

Iron bearing particles from diesel engines using fuel additives have been reported to consist of nanoscale primary particles (5–10 nm) incorporated within complex carbon soot agglomerates. Particles of Fe included in carbonaceous soot in this fashion have not been observed in our ambient measurements, most Fe particles appearing in the form of agglomerates with similar particles, although some agglomerates are attached to larger particles. It has been reported that at higher doping levels, primary particles become larger and iron nanoparticle clusters begin to form (Miller et al., 2007). Nash et al. (2013) reported that iron represents around 0.1% of the total mass of diesel soot from undoped fuel. Introducing iron into the fuel changes the size distribution by increasing the nanoparticle component. In small particles (18 nm mean) spherical nanoparticles and irregular clusters are present. At 100 nm mean

Table 2
Mean diameter (±s.d.) of primary spherules in iron phase particles.

Oxide	High-Fe mean (nm)	High-Fe stdev	N	Moderate-Fe mean (nm)	Moderate-Fe stdev	N
FeO	26.35	0.00	n = 1	18.77	0.00	n = 1
Fe_3O_4	26.97	20.88	n = 8	20.49	1.13	n = 3
γ-Fe_2O_3	32.28	22.34	n = 11	22.97	7.98	n = 11
α-Fe_2O_3	13.14	11.61	n = 5	33.56	39.90	n = 6

Table 3
Primary particle and agglomerate sizing data.

	High Fe			Moderate Fe		
	Combined	Birmingham	Newcastle	Combined	Birmingham	Newcastle
Primary particle size (nm)	24	24.7	18.3	14.9	34.2	12.1
Cluster size (nm)	400	690	248	204	177	225
Total number 1° particles in analysed areas	225	74	151	107	25	92
Number of spectra	48	12	36	28	13	15

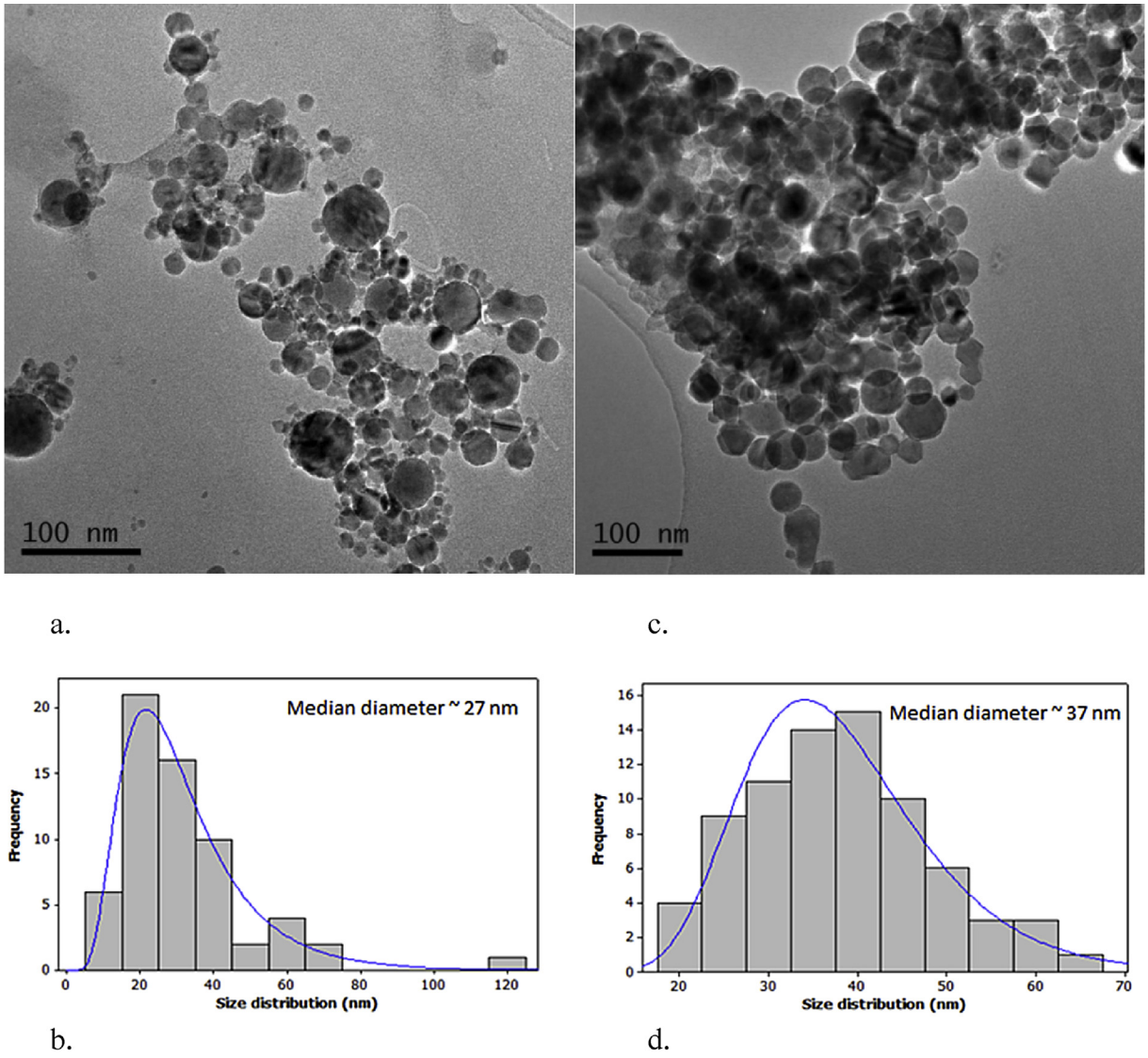

Fig. 7. Bright-field TEM images of (a) high-Fe and (c) moderate-Fe agglomerates with size distribution plots for primary particles of (b) high-Fe and (d) moderate-Fe below.

diameter, iron is mostly present as inclusions and surface deposits on carbon soot particles (Nash et al., 2013). By contrast the majority of Fe oxide particles we have observed in the environment are agglomerates of Fe particles, not inclusions or surface deposits. This suggests that they form in an iron-rich environment, rather than having coagulated in the atmosphere where particle composition is very diverse.

4. Conclusions

It has been confirmed that iron particles are present in submicrometre atmospheric particulate matter in urban environments, mostly in the form of agglomerations of nano-scale primary particles formed of iron oxides. There are a range of different internally mixed composition types incorporating a number of different alloying elements which fall into two main categories, a high-Fe class where Fe accounts for ~90% of the total weight (excluding C and O), and a moderate-Fe class where Fe accounts for ~75% of the total weight (excluding C and O). This indicates a range of sources may be contributing iron particles to the environment, but it is not easy to assign sources to the ambient particles.

Comparing the ambient particles to particles observed in

previous studies, both direct from sources and in the environment, leads to an inconclusive picture concerning potential sources. Given that similar particles have been observed at two widely separated sites in which road traffic is the most important common source, it would be reasonable to assume that road traffic is the source, and the spherical/near-spherical morphology probably indicates an origin in high-temperature processes in an iron-rich environment. This seems most likely to be associated with the engine cylinder or the brakes. No firm conclusion can be drawn over the presence of the two particle types, but presumably these reflect the composition of the bulk material (e.g. engine block) from which they derive.

Acknowledgements

The authors acknowledge the Natural Environment Research Council (NERC), Medical Research Council (MRC), Department of Health (DH), Economic and Social Research Council (ESRC), and Department for Environment, Food and Rural Affairs (DEFRA), for the funding received for this project through the Environmental Exposures & Health Initiative (EEHI) (Grant No. NE/I008314/1). SuperSTEM is the National Facility for Aberration Corrected Electron Microscopy funded by the Engineering and Physical Sciences Research Council (EPSRC).

Appendix A. Supplementary data

Supplementary data related to this article can be found at http://dx.doi.org/10.1016/j.atmosenv.2016.05.040.

References

Adachi, K., Tainosho, Y., 2004. Characterization of heavy metal particles embedded in tire dust. Environ. Int. 30, 1009–1017.
Amato, F., Pandolfi, M., Moreno, T., Furger, M., Pey, J., Alastuey, A., Bukowiecki, N., Prevot, A.S.H., Baltensperger, U., Querol, X., 2011. Sources and variability of inhalable road dust particles in three European cities. Atmos. Environ. 45, 6777–6787.
Bardelli, F., Cattaruzza, E., Gonella, F., Rampazzo, G., Valatto, G., 2011. Characterization of road dust collected in *Traforo del San Bernardo* highway tunnel: Fe and Mn speciation. Atmos. Environ. 45, 6459–6468.
Buonanno, G., Stabile, L., Avino, P., Belluso, E., 2011. Chemical, dimensional and morphological ultrafine particle characterization from a waste-to-energy plant. Waste Manag. 31, 2253–2262.
Chen, Y., Shah, N., Huggins, F.E., Huffman, G.P., 2006. Microanalysis of ambient particles from Lexington, KY, by electron microscopy. Atmos. Environ. 40, 651–663.
Cernuschi, S., Giugliano, M., Ozgen, S., Consonni, S., 2012. Number concentration and chemical composition of ultrafine and nanoparticles from WTE (waste to energy) plants. Sci. Total Environ. 420, 319–326.
d'Acapito, F., Mazziotti Tagliani, S., Di Benedetto, F., Gianfagna, A., 2014. Local order and valence state of Fe in urban suspended particulate matter. Atmos. Environ. 99, 582–586.
Erel, Y., Pehkonen, S.O., Hoffmann, M.R., 1993. Redox chemistry of iron in fog and stratus clouds. J. Geophys. Res. Atmos. 98, 18423–18434.
Fittschen, U.E.A., Meirer, F., Streli, C., Wobrauschek, P., Thiele, J., Falkenberg, G., Pepponi, G., 2008. Characterization of atmospheric aerosols using Synchroton radiation total reflection X-ray fluorescence and Fe K-edge total reflection X-ray fluorescence-X-ray absorption near-edge structure. Spectrochim. Acta Part B At. Spectrosc. 63, 1489–1495.
Gantt, B., Hoque, S., Willis, R.D., Fahey, K.M., Delgado-Saborit, J.M., Harrison, R.M., Erdakos, G.B., Bhave, P.V., Zhang, K.M., Kovalcik, K., Pye, H.O.T., 2014. Near-Road modeling and measurement of cerium-containing particles generated by nanoparticle diesel fuel additive use. Environ. Sci. Technol. 48, 10607–10613.
Gantt, B., Hoque, S., Fahey, K.M., Willis, R.D., Delgado-Saborit, J.M., Harrison, R.M., Zhang, K.M., Jefferson, D.A., Kalberer, M., Bunker, K.L., Conny, J.M., Bhave, P.V., Weinstein, J.P., Pye, H.O.T., 2015. Factors affecting the ambient physicochemical properties of cerium-containing particles generated by nanoparticle diesel fuel additive use. Aerosol Sci. Technol. 49, 371–380.
Gietl, J.K., Lawrence, R., Thorpe, A.J., Harrison, R.M., 2010. Identification of brake wear particles and derivation of a quantitative tracer for brake dust at a major road. Atmos. Environ. 44, 141–146.
Grgić, I., Dovžan, A., Hudnik, V., 1996. The role of atmospheric aerosols in SO2 oxidation: catalytic effect of iron in the presence of organic ligands. J. Aerosol Sci. 27 (Suppl. 1), S657–S658.
Gurzau, E.S., Neagu, C., Gurzau, A.E., 2003. Essential metals—case study on iron. Ecotoxicol. Environ. Saf. 56, 190–200.
Harper, S.L., Walling, J.F., Holland, D.M., Pranger, L.J., 1983. Simplex optimization of multielement ultrasonic extraction of atmospheric particulates. Anal. Chem. 55, 1553–1557.
Harrison, R.M., Jones, A.M., Gietl, J., Yin, J., Green, D.C., 2012. Estimation of the contributions of brake dust, tire wear, and resuspension to nonexhaust traffic particles derived from atmospheric measurements. Environ. Sci. Technol. 46, 6523–6529.
Harrison, R.M., Jones, A.M., Lawrence, R.G., 2004. Major component composition of PM10 and PM2.5 from roadside and urban background sites. Atmos. Environ. 38, 4531–4538.
Kopcewicz, B., Kopcewicz, M., 2001. Long-term measurements of iron-containing aerosols by Mössbauer spectroscopy in Poland. Atmos. Environ. 35, 3739–3747.
Kukutschová, J., Moravec, P., Tomášek, V., Matějka, V., Smolík, J., Schwarz, J., Seidlerová, J., Šafářová, K., Filip, P., 2011. On airborne nano/micro-sized wear particles released from low-metallic automotive brakes. Environ. Pollut. 159, 998–1006.
Lee, D., Miller, A., Kittelson, D., Zachariah, M.R., 2006. Characterization of metal-bearing diesel nanoparticles using single-particle mass spectrometry. J. Aerosol Sci. 37, 88–110.
Liati, A., Dimopoulos Eggenschwiler, P., Müller Gubler, E., Schreiber, D., Aguirre, M., 2012. Investigation of diesel ash particulate matter: a scanning electron microscope and transmission electron microscope study. Atmos. Environ. 49, 391–402.
Liati, A., Pandurangi, S.S., Boulouchos, K., Schreiber, D., Arroyo Rojas Dasilva, Y., 2015. Metal nanoparticles in diesel exhaust derived by in-cylinder melting of detached engine fragments. Atmos. Environ. 101, 34–40.
Linak, W.P., Yoo, J.-I., Wasson, S.J., Zhu, W., Wendt, J.O.L., Huggins, F.E., Chen, Y., Shah, N., Huffman, G.P., Gilmour, M.I., 2007. Ultrafine ash aerosols from coal combustion: characterization and health effects. Proc. Combust. Inst. 31, 1929–1937.
Mahmoudi, M., Hofmann, H., Rothen-Rutishauser, R., Petri-Fink, A., 2012. Assessing the in vitro and in vivo toxicity of superparamagnetic iron oxide nanoparticles. Chem. Rev. 112, 2323–2338.
Mahowald, N.M., Baker, A.R., Bergametti, G., Brooks, N., Duce, R.A., Jickells, T.D., Kubilay, N., Prospero, J.M., Tegen, I., 2005. Atmospheric global dust cycle and iron inputs to the ocean. Glob. Biogeochem. Cycles 19, GB4025.
Marris, H., Deboudt, K., Flament, P., Grobéty, B., Gieré, R., 2013. Fe and Mn oxidation states by TEM-EELS in fine-particle emissions from a Fe–Mn alloy making plant. Environ. Sci. Technol. 47, 10832–10840.
Miller, A., Ahlstrand, G., Kittelson, D., Zachariah, M., 2007. The fate of metal (Fe) during diesel combustion: morphology, chemistry, and formation pathways of nanoparticles. Combust. Flame 149, 129–143.
Moldanová, J., Fridell, E., Popovicheva, O., Demirdjian, B., Tishkova, V., Faccinetto, A., Focsa, C., 2009. Characterisation of particulate matter and gaseous emissions from a large ship diesel engine. Atmos. Environ. 43, 2632–2641.
Mosleh, M., Blau, P.J., Dumitrescu, D., 2004. Characteristics and morphology of wear particles from laboratory testing of disk brake materials. Wear 256, 1128–1134.
Nash, D.G., Swanson, N.B., Preston, W.T., Yelverton, T.L.B., Roberts, W.L., Wendt, J.O.L., Linak, W.P., 2013. Environmental implications of iron fuel borne catalysts and their effects on diesel particulate formation and composition. J. Aerosol Sci. 58, 50–61.
Nico, P.S., Kumfer, B.M., Kennedy, I.M., Anastasio, C., 2009. Redox dynamics of mixed metal (Mn, Cr, and Fe) ultrafine particles. Aerosol Sci. Technol. 43, 60–70.
Patel, M., Azanza Ricardo, C.L., Scardi, P., Aswath, P.B., 2012. Morphology, structure and chemistry of extracted diesel soot—Part I: transmission electron microscopy, Raman spectroscopy, X-ray photoelectron spectroscopy and synchrotron X-ray diffraction study. Tribol. Int. 52, 29–39.
Reinard, M.S., Adou, K., Martini, J.M., Johnston, M.V., 2007. Source characterization and identification by real-time single particle mass spectrometry. Atmos. Environ. 41, 9397–9409.
Sanderson, P., Delgado-Saborit, J.M., Harrison, R.M., 2014. A review of chemical and physical characterisation of atmospheric metallic nanoparticles. Atmos. Environ. 94, 353–365.
Song, J., Wang, J., Boehman, A.L., 2006. The role of fuel-borne catalyst in diesel particulate oxidation behavior. Combust. Flame 146, 73–84.
Thorpe, A., Harrison, R.M., 2008. Sources and properties of non-exhaust particulate matter from road traffic: a review. Sci. Total Environ. 400, 270–282.
Zhang, G., Bi, X., Lou, S., Li, L., Wang, H., Wang, X., Zhou, Z., Sheng, G., Fu, J., Chen, C., 2014. Source and mixing state of iron-containing particles in Shanghai by individual particle analysis. Chemosphere 95, 9–16.
Zhou, Y.-M., Zhong, C.-Y., Kennedy, I.M., Pinkerton, K.E., 2003. Pulmonary responses of acute exposure to ultrafine iron particles in health adult rats. Environ. Toxicol. 18, 227–235.